Solution structure of human thioredoxin in a mixed disulfide intermediate complex with its target peptide from the transcription factor NFκB

Jun Qin, G Marius Clore*, WM Poindexter Kennedy, Jeffrey R Huth and Angela M Gronenborn*

Laboratory of Chemical Physics, Building 5, National Institute of Diabetes and Digestive and Kidney Diseases, National Institutes of Health, Bethesda, MD 20892-0520, USA

Background: Human thioredoxin is a 12 kDa cellular redox protein that plays a key role in maintaining the redox environment of the cell. It has recently been shown to be responsible for activating the DNA-binding properties of the cellular transcription factor, NFκB, by reducing a disulfide bond involving Cys62 of the p50 subunit. Using multidimensional heteronuclear-edited and heteronuclear-filtered NMR spectroscopy, we have solved the solution structure of a complex of human thioredoxin and a 13-residue peptide extending from residues 56–68 of p50, representing a kinetically stable mixed disulfide intermediate along the reaction pathway.

Results: The NFκB peptide is located in a long boot-shaped cleft on the surface of human thioredoxin delineated by the active-site loop, helices α2, α3 and α4, and strands β3 and β4. The peptide adopts a crescent-like conformation with a smooth 110° bend centered around residue 60 which permits it to follow the path of the cleft.

Conclusions: In addition to the intermolecular disulfide bridge between Cys32 of human thioredoxin and Cys62 of the peptide, the complex is stabilized by numerous hydrogen-bonding, electrostatic and hydrophobic interactions which involve residues 57–65 of the NFκB peptide and confer substrate specificity. These structural features permit one to suggest the specificity requirements for human thioredoxin-catalyzed disulfide bond reduction of proteins.

Structure 15 March 1995, **3**:289–297

Key words: disulfide-bonded intermediate, human thioredoxin, transcription factor NFκB

Introduction

A growing body of evidence over recent years has demonstrated that the DNA-binding properties of a number of eukaryotic transcription factors are regulated by a thiol–redox control mechanism involving the reduction of a specific cysteine residue [1–9]. The best studied examples include, NFκB, AP-1, TFIIIC, BZLF1 and Myb. In the case of NFκB, it has been shown both *in vitro* and *in vivo* that human thioredoxin (hTRX), a 12 kDa cellular redox protein, is responsible for the activation of its DNA-binding properties by specifically reducing a disulfide bond involving a critical cysteine residue at position 62 of the p50 subunit [1–3].

Thioredoxins are found in many organisms ranging from prokaryotes to eukaryotes and play a key role in maintaining the redox environment of the cell [10], acting as potent reducing agents for disulfide bonds in many proteins [11]. A human protein with thioredoxin-like activity was first identified in human platelet extracts [12] and subsequently shown to be present in human cultured fibroblasts [13]. Approximately 10 years later, hTRX was identified independently as a highly expressed cytokine-like factor in activated T and B cell lines that induced the production of the interleukin-2 receptor α chain and interleukin-2 [14–20], both of which are under the transcriptional control of NFκB [21].

NFκB is an important cellular transcription factor [22–25] that regulates not only a wide variety of cellular genes, particularly those involved in host defense, but also a number of viral genes including those of the proviral form of HIV-1 [26,27]. We have therefore undertaken a structural study to investigate the molecular basis of the hTRX-mediated activation of NFκB. To this end we have determined the solution structure of a disulfide-bonded complex between hTRX and a 13-residue peptide comprising residues 56–68 of the p50 subunit of NFκB and encompassing Cys62. This portion of NFκB, which is located in the L1 loop, makes numerous contacts to DNA in the crystal structure of the NFκB p50 homodimer bound to a κB site [28,29]. The structure of the hTRX–NFkB peptide complex also represents the first structure of a mixed disulfide intermediate on the reaction pathway involving thioredoxin from any species and thus sheds light on the specificity of thioredoxin-catalyzed disulfide bond reduction.

Results and discussion

Structure determination

The proposed mechanism of disulfide bond reduction by thioredoxin involves nucleophilic attack by the highly reactive Cys32 thiolate anion (pK_a ~6.3 in hTRX [30]) of the reduced species on a disulfide-containing substrate,

*Corresponding authors.

producing a mixed disulfide intermediate (that is, an intermediate containing an intermolecular disulfide bond), followed by attack of the thiolate of Cys35 (pK_a ~7.5–8.6 in hTRX [30]) to yield a reduced substrate and oxidized thioredoxin [31]. We therefore trapped a kinetically stable mixed disulfide intermediate (that is an intermediate containing an intermolecular disulfide bond) of hTRX and the NFκB peptide using the quadruple Cys→Ala mutant (C35A, C62A, C69A and C73A) of hTRX which retains the reactive Cys32. The mutations Cys62→Ala, Cys69→Ala and Cys73→Ala were previously introduced into the protein in our study of the structures of reduced and oxidized hTRX to circumvent any problems arising from intermolecular disulfide bond formation involving the three free non-active-site cysteine residues (Cys62, Cys69 and Cys73) upon oxidation [32]. The mixed disulfide intermediate was formed by reacting the mutated hTRX with the NFκB peptide at pH 8, and purified by high-performance liquid chromatography (HPLC). A similar strategy was employed to determine the structure of a mixed disulfide intermediate of glutaredoxin and glutathione [33,34].

The structure was solved by means of multidimensional double and triple resonance heteronuclear-filtered and heteronuclear-edited NMR spectroscopy making use of the NFκB peptide at natural isotopic abundance (i.e. ^{12}C and ^{14}N), and uniformly (>95%) ^{15}N and $^{15}N/^{13}C$-labeled hTRX. An example of the quality of the data is shown in Fig. 1 which illustrates strips taken from the three-dimensional (3D) ^{13}C edited(F_2)/$^{12}C(F_3)$-filtered nuclear Overhauser enhancement (NOE) spectrum illustrating short interproton distance contacts specifically between ^{13}C-attached protons of hTRX and ^{12}C-attached protons of the unlabeled NFκB peptide. The structural statistics for the final ensemble of 60 simulated annealing structures, calculated on the basis of 3169 experimental NMR restraints, are summarized in Table 1, and a stereoview of a best fit superposition of the backbone atoms and ordered side chains is shown in Fig. 2.

The restraints comprise 2582 approximate distance restraints as follows: 2357 intramolecular hTRX interproton distance restraints [subdivided into 690 intra-residue restraints, and 503 sequential ($|i-j|=1$), 437 short-range ($1<|i-j|\leq 5$) and 727 long-range ($|i-j|>5$) inter-residue restraints], 115 intramolecular NFκB peptide interproton distance restraints (subdivided into 64 intra-residue restraints and 38 sequential and 13 medium-range inter-residue restraints), 74 intermolecular hTRX–NFκB interproton distance restraints, and 36 distance restraints for 18 hydrogen bonds in hTRX. These were supplemented by 300 torsion angle restraints (104 ϕ, 76 ψ, 78 $\chi 1$ and 31 $\chi 2$ restraints for hTRX, and 7 $\chi 1$ and 4 $\chi 2$ restraints for the NFκB peptide), 88 $^3J_{HN\alpha}$ coupling constant restraints, and 102 $^{13}C\alpha$ and 97 $^{13}C\beta$ chemical shift restraints. The N-terminal (residue 56) and C-terminal (residue 68) residues of the NFκB peptide, which are not in contact with hTRX, are disordered. The remainder of the complex is very well defined with a precision [defined as the average root mean square (rms) difference between the individual simulated annealing structures and the mean coordinate positions] of 0.21±0.02 Å for the backbone atoms, 0.57–0.03 Å for all atoms and 0.34±0.03 Å for all ordered atoms (Table 2).

Description of the structure

The overall structure of hTRX in the complex is similar to that of oxidized and reduced hTRX [32] and is characterized by a five-stranded β-sheet (residues 1–5, 22–28, 53–59, 75–81 and 84–91) arranged in a –2x, +1x, –2, –1 topology [35] and surrounded by four α-helices (residues 7–17, 33–49, 62–70 and 94–105). The backbone atomic rms difference between the mean coordinates of the hTRX–NFκB complex and oxidized hTRX, the hTRX–NFκB complex and reduced hTRX, and reduced and oxidized hTRX are 0.64 Å, 0.83 Å and 0.86 Å, and the corresponding values for all atoms are 0.78 Å, 1.0 Å and 1.0 Å, respectively. As the precision of the solution structures of reduced and oxidized hTRX [32] is comparable to that of the complex reported here,

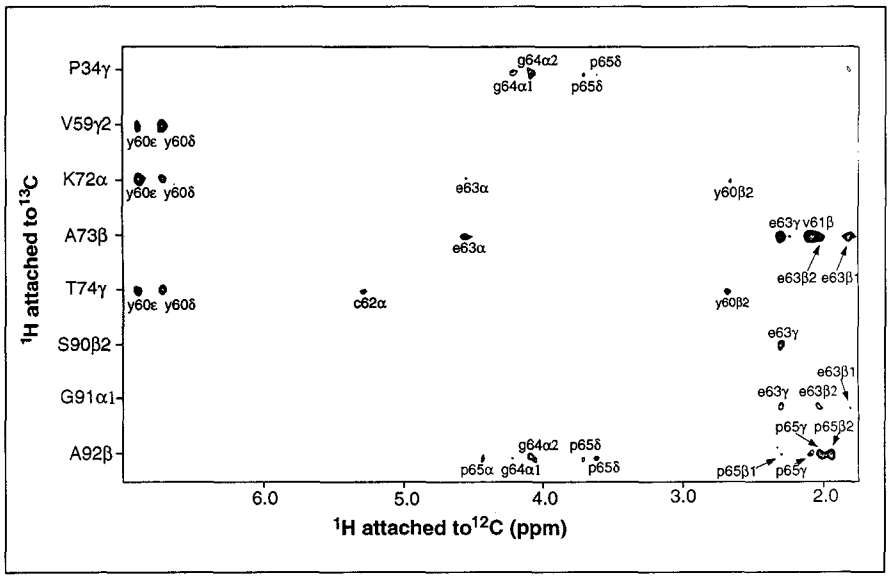

Fig. 1. Composite of ^{13}C–H strips taken from the 120 ms mixing time 600 MHz 3D $^{13}C(F_2)$-edited/$^{12}C(F_3)$-filtered NOE spectrum of the hTRX–NFκB peptide complex, illustrating NOEs between protons of the unlabeled peptide (attached to ^{12}C along the F_3 axis) and protons of labeled hTRX (attached to ^{13}C). Residues of hTRX and the NFκB peptide are indicated by upper-case and lower-case letters, respectively.

Table 1. Structural statistics.[a]

	<SA>	$(\overline{SA})_r$
Rmsds from experimental distance restraints (Å)[b]		
All (2582)	0.026±0.001	0.026
Intramolecular hTRX interproton distances		
inter-residue sequential ($\|i-j\|=1$) (503)	0.018±0.003	0.016
inter-residue short range ($1<\|i-j\|\leq 5$) (437)	0.034±0.003	0.039
inter-residue long range ($\|i-j\|>5$) (727)	0.027±0.002	0.029
intra-residue (690)	0.019±0.001	0.014
Intramolecular NFκB peptide interproton distances (115)	0.032±0.003	0.032
Intermolecular hTRX–NFκB interproton distances (74)	0.053±0.006	0.054
hTRX hydrogen-bond restraints (36)	0.024±0.007	0.026
Rmsds from complete cross-validated experimental distances (Å)[c]	0.15±0.06	
Rmsds from $^3J_{HN\alpha}$ coupling constants (Hz) (88)[b]	0.41±0.03	0.47
Rmsds from experimental dihedral restraints (°) (300)[b]	0.38±0.05	0.50
Rmsds from experimental secondary shifts (ppm)		
$^{13}C\alpha$ (102)	1.02±0.02	1.07
$^{13}C\beta$ (97)	1.10±0.02	1.12
Deviations from idealized covalent geometry		
Bonds (Å) (1865)	0.004±0.0003	0.005
Angles (°) (3360)	0.594±0.014	0.658
Impropers (°) (969)[d]	0.407±0.028	0.531
E_{L-J} (kcal mol^{-1})[e]	−576±10	−561

[a]The notation of the NMR structures is as follows: <SA> are the final 60 simulated annealing structures; $\overline{SA}$ is the mean structure obtained by averaging the coordinates of the individual SA structures best fitted to each other (excluding residues 56 and 68 of the NFκB peptide); $(\overline{SA})_r$ is the restrained minimized mean structure obtained by restrained regularization of the mean structure $\overline{SA}$. The number of terms for the various restraints is given in parentheses and applies to the entire complex. [b]None of the structures exhibits distance violations >0.3 Å, dihedral angle violations >5°, or $^3J_{HN\alpha}$ coupling constant violations >2 Hz; and there are no systematic interproton distance violations between 0.1 Å and 0.3 Å among the ensemble of calculated structures. For each backbone hydrogen bond there are two distance restraints: r_{NH-O}, 1.7–2.5 Å; r_{N-O}, 2.3–3.5 Å. [c]The value quoted represents the average rmsd for all test sets which comprise a different subset (10%) of the data in each calculation. [d]The improper torsion restraints serve to maintain planarity and chirality. All peptide bonds were constrained to be planar and *trans* with the exception of the peptide bond between Thr74 and Pro75 which is in the *cis* conformation [32]. [e]E_{L-J} is the Lennard-Jones van der Waals energy calculated with the CHARMM [81] empirical energy function and is not included in the target function for simulated annealing or restrained minimization.

the differences between the structures, albeit small, are significant. Thus, the overall structure of hTRX in the complex is slightly closer to that of the oxidized species than to that of reduced hTRX.

To facilitate discussion, we denote the residue numbering of the NFκB peptide as follows: S_0 represents the disulfide-bonded cysteine, and negative and positive numbers indicate residues N-terminal and C-terminal to this cysteine, respectively. Residues S_{-5}(Arg57) to S_{+3}(Pro65) are in contact with hTRX. They bind in a crescent-like conformation to a boot-shaped cleft on the surface of hTRX, which is 8–10 Å wide and 5–6 Å deep, with the shank and foot of the boot ~18 Å and 15 Å in length, respectively (Fig. 3). The angle between the long axes of the boot and shank is ~110°. In the views shown in Figs 3 and 4a, the borders of the cleft are formed by the N terminus of helix α2 and the C terminus of helix α4 (located at the top of hTRX), the active-site loop (residues 31–36) and the C terminus of strand β3 (on the left-hand side), and by helix α3, the loop connecting helix α3 and strand β4, and strand β5 (on the right-hand side). Residues S_{-5}(Arg57)–S_{-3}(Arg59) are located in the foot of the cleft, with residues S_{-2}(Tyr60)–S_{+3}(Pro65) located in the shank. The side chain of the S_{-3}(Arg59) residue points directly into the heel of the cleft. The chain of the NFκB peptide follows the cleft by bending smoothly through 110° with the bend centered on the S_{-2}(Tyr60) residue. The S_{+3}(Pro65) residue abuts the uppermost point of the cleft where the cleft boundaries force the chain of the NFκB peptide to reverse direction resulting in a turn centered on residues S_{+3}(Pro65) and S_{+4}(Ser66). This turn is accompanied by a backbone carbonyl to amide hydrogen bond between the S_{+2}(Gly64) and S_{+5}(His67) residues. The polypeptide backbone of the NFκB peptide is defined up to the Cα carbon of the S_{+5} residue; the side chain of this residue makes no contact with hTRX and is disordered.

The disulfide bridge between Cys32 of hTRX and S_0(Cys62) has a right-handed *trans-trans-gauche*(+)-*trans-gauche*(−) conformation with a Cα–Cα separation of 6.8 Å, similar to that of the disulfides that span the β-barrels in immunoglobulins [35]. In addition to the covalent linkage afforded by the disulfide bridge, the complex between the NFκB peptide and hTRX is stabilized by numerous non-covalent interactions that confer specificity to substrate binding. These are illustrated in detail in Fig. 4.

There are three backbone hydrogen bonds between the NFκB peptide and hTRX in the immediate vicinity of the S_0(Cys62) residue. In particular, the backbone carbonyl of the S_{-2}(Tyr60) residue is hydrogen bonded to the backbone amide of Thr74, and the backbone amide and carbonyl of the S_{+1}(Glu63) residue are hydrogen bonded to the backbone carbonyl of Thr74 and the backbone amide of Ala92, respectively. There are five electrostatic interactions involving three side chains of the NFκB peptide. The guanidinium group of the S_{-5}(Arg57) residue forms a salt bridge with the side-chain carboxylates of Asp58 and Asp61; the guanidinium group of the S_{-3}(Arg59) residue is hydrogen bonded to the side-chain carbonyl of Gln63 and the hydroxyl group of Ser67; and the carboxylate of the S_{+1}(Glu63) residue forms a hydrogen bond with the hydroxyl group of Ser90. It should be noted that, on the basis of pH titration data (JQ, GMC and AMG, unpublished data), the carboxylate groups of Asp58 and Asp61 are negatively charged at the pH of 4.4 employed in this study. In addition, it seems likely that the hydroxyl group of the S_{-2}(Tyr60) residue is hydrogen bonded to the backbone carbonyl of Phe27 via a bridging water molecule. Finally, an extensive set of hydrophobic interactions is observed. The aromatic ring of the S_{-4}(Phe58) residue is stacked against the six-membered ring of Trp31; the aliphatic portion of the side chain of

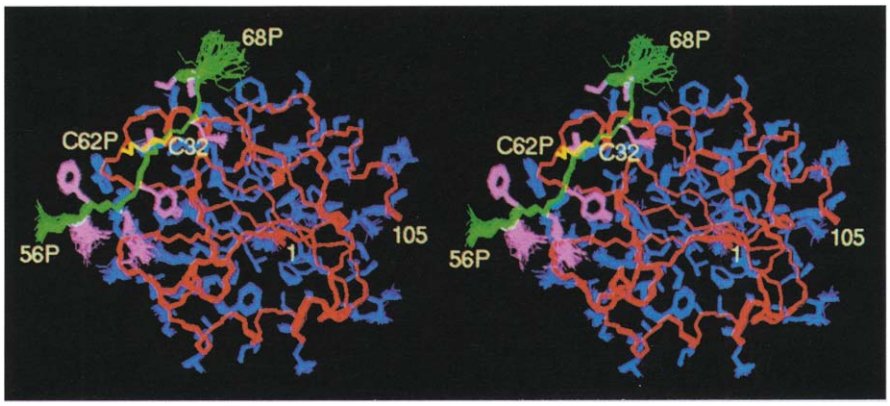

Fig. 2. Stereoview showing a best fit superposition of the backbone N, Cα, C atoms and ordered side chains of the 60 simulated annealing structures of the hTRX–NFκB complex. The backbone and side chains of hTRX are shown in red and blue, respectively; the backbone and side chains of the NFκB peptide are shown in green and pink, respectively, and the disulfide bond between Cys32 of hTRX and Cys62 of the NFκB peptide is shown in yellow. P designates a residue from the NFκB peptide. (Figure generated with the program AVS-X-PLOR [82].)

Table 2. Atomic root mean square differences.

	Backbone atoms	All atoms	All ordered atoms[b]
<SA> *versus* $\overline{SA}$[a]	0.21±0.02	0.57±0.03	0.34±0.03
<SA> *versus* $(\overline{SA})_r$	0.097	0.33	0.20
$(\overline{SA})_r$ *versus* $\overline{SA}$	0.23±0.02	0.65±0.04	0.40±0.03

[a]The notation of the structures is given in the footnote of Table 1. [b]The atoms that do not exhibit conformational disorder comprise all N, Cα, C, O and Cβ atoms of residues 1–105 of hTRX and 57–67 of the NKκB peptide; the complete hTRX side chains of residues 2, 5, 7–9, 10, 11, 14, 15, 17–19, 22–25, 27, 29–35, 38, 40–43, 45, 46, 49–55, 57, 59, 60, 62, 65–67, 69, 71, 73–80, 83, 86–92, 97 and 99–105; the complete side chains of the NFκB peptide excluding those of residues 56 and 67; and the hTRX side chains of M1, Q12, S28, M37, S44 and E88 up to Cβ, K3, E6, E13, D16, D20, D26, E47, D58, D61, D64, K72, Q84, N93, K94, E95 and E98 up to Cγ, and Q4, K8, K21, K36, K39, K48, E56, E68, E70, K81, K85 and K96 up to Cδ.

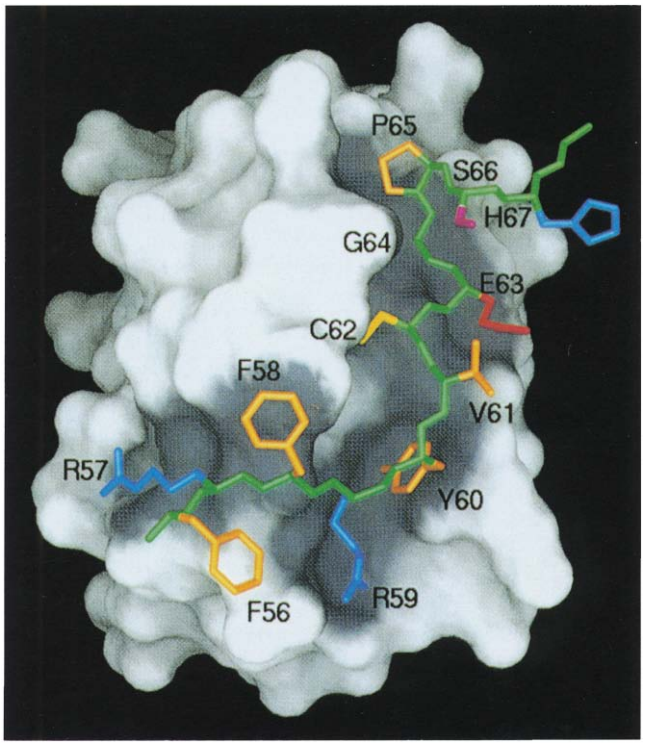

Fig. 3. View of the molecular surface of hTRX illustrating the cleft in which the NFκB peptide is located. The degree of curvature of the molecular surface is color coded from white (convex) to dark gray (concave). Hence the cleft is visualized as the contiguous boot-shaped gray region on the surface of hTRX. The backbone of the peptide is shown in green, and side chains are colored as follows: Phe, Tyr, Val, Pro and Cys in yellow; Arg and His in blue; Glu in red and Ser in magenta. Note that the side chains of Phe56 and His67 of the bound NFκB peptide are disordered in solution. (Figure generated with the program GRASP [83].)

the S_{-3}(Arg59) residue is in contact with the methyl groups of Val59 and Ala66; the aromatic ring of the S_{-2}(Tyr60) residue is in contact with the methyl groups of Val59, Ala66, Val71 and Thr74; the β-methine of the S_{-1}(Val61) residue and the β- and γ-methylene groups of the S_{+1}(Glu63) residue are in contact with Ala73; the disulfide bridge involving the S_0(Cys62) residue is in contact with the methyl group of Ala35 and the side chains of Pro34 and Pro75; the S_{+2}(Gly64) residue is in contact with Pro34; and finally, the S_{+5}(Pro65) residue is in contact with Pro34, the Cδ-methyl and Cγ-methylene groups of Ile38, the Cβ- and Cγ-methylene groups of Met37, and the methyl group of Ala92. It is worth noting that the variant of hTRX employed in this study has a threonine at position 74 [36], whereas another variant has a methionine at this position [18]. This difference should have no effect on the hydrophobic interaction between the residue at position 74 and the aromatic ring of the S_{-2}(Tyr60) residue of the peptide.

The importance of these hydrophobic interactions can be ascertained by calculating the solvation free energy (SFE) of folding [37] of the complex relative to its individual components. Formation of the complex is associated with a decrease of 768 Å^2 and 535 Å^2 in the solvent accessible surface area of the NFκB peptide and hTRX, respectively, which corresponds to a decrease in the calculated SFE of folding of 6.2 kcal mol^{-1} and 6.3 kcal mol^{-1}, respectively. Indeed, 58% of the surface of the NFκB peptide in contact with hTRX is buried compared with 6% for the free peptide (in the same conformation as in the complex). Thus, the geometric and chemical characteristics of the hTRX–NFκB peptide interface are similar to those of other high-affinity protein–peptide interactions [38–40]. We would therefore predict that the affinity of the NFκB peptide for hTRX could remain high even in the absence of a disulfide

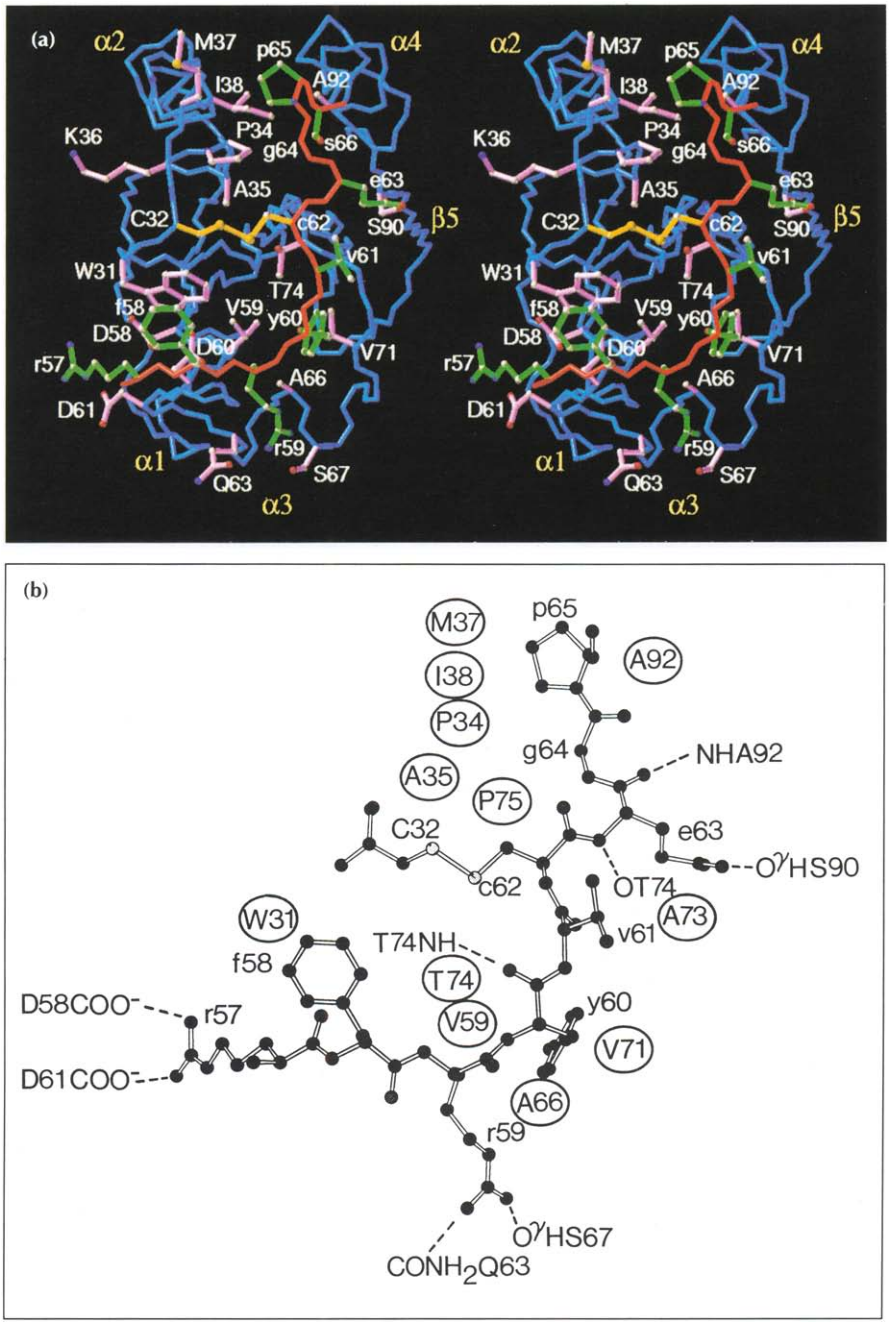

Fig. 4. Interactions between the NFκB peptide and hTRX. Only residues 57–65 of the NFκB peptide, which are in contact with hTRX, are shown, and the residues of the peptide and hTRX are depicted by lower-case and upper-case letters, respectively. **(a)** Stereoview of the backbone (N, Cα, C) of hTRX (blue) and the NFκB peptide (red). The side chains of hTRX and the NFκB peptide at the interface of the complex are shown in pink and green, respectively, and the disulfide bond between Cys32 of hTRX and Cys62 of the NFκB peptide is shown in yellow. (Figure generated with the program VISP [84].) **(b)** Schematic representation of the hTRX–NFκB peptide complex. Residues of hTRX involved in hydrophobic interactions with the peptide are shown circled, and the dashed lines indicate hydrogen bonds, salt bridges or electrostatic interactions. (The NFκB peptide chain was generated by the program MOLSCRIPT [85].)

bridge (for example if either Cys32 or S_0(Cys62) were mutated to alanine).

Following attack on the Cys32–S_0(Cys62) disulfide bridge by the Cys35 thiolate anion (which, judging from the position of Ala35 in the present structure, would be positioned directly on top of the disulfide bridge) and the subsequent formation of an intramolecular Cys32–Cys35 disulfide bond, it is clear that the affinity of the peptide for thioredoxin would have to be much reduced to permit its release. We suggest that this is accomplished as follows: formation of the intramolecular disulfide bridge will necessarily alter the positioning of the S_0(Cys62) residue to avoid steric clash with the Cys32-Cys35 intramolecular disulfide bridge. This in turn is likely to disrupt the backbone hydrogen bonds involving the S_{-1} and S_{+1} residues, thereby reducing the affinity of the peptide for oxidized hTRX. In this regard, it is interesting to note that the aperture of the cleft formed by the active site and the two opposing loops (residues 74–76 and 90–92) as measured by the Cα–Cα distances between Cys/Ala35, Pro75 and Ala92 is 10–20% wider in the oxidized protein than in the complex. We should also note that in the intact system, NFκB itself may undergo a conformational change upon reduction that facilitates its release.

Specificity requirements of hTRX

The structure of the hTRX–NFκB peptide complex provides insight into the specificity requirements of hTRX for its target disulfide bonds in proteins. The identity of the S_{-1} residue is unlikely to influence binding

as its side chain is directed into the solvent and only makes contact with hTRX up to the level of the β-carbon. All the remaining side chains, however, from S_{-5} to S_{-2} and from S_{+1} to S_{+3}, play a role in stabilizing the encounter complex through non-covalent interactions. The S_{-5} residue should be positively charged (arginine or lysine) to permit interaction with the carboxylates of Asp58 and Asp61. The S_{-3} residue should have a long hydrophobic side chain together with a functional group to permit hydrogen bonding to the side chains of Gln63 and/or Ser67 (for example, arginine, lysine or glutamine). The side chains of the S_{-4} and S_{+3} residues should either be hydrophobic (aromatic, leucine, isoleucine, valine or methionine) or have a long hydrophobic component (arginine, lysine). The S_{-2} residue should be hydrophobic (aromatic, leucine, isoleucine, valine or methionine) as it is buried deep within the interface of the complex. The S_{+1} residue should be hydrophilic and capable of interacting with Ser90 (for example, glutamate, glutamine, arginine or lysine). Finally, the S_{+2} residue should be small and hydrophobic to prevent steric clashes (glycine or alanine).

It is interesting to note that the S_{-5} to S_{+3} sequence of the p50 subunit is highly preserved in the NFκB/Rel/Dorsal transcription factor family which includes p50, p49, p65, Rel, I-Rel and Dorsal [41,42]. The S_{-5} residue is conserved in all members of the family with the exception of I-Rel where arginine is replaced by proline; the S_{-4}, S_{-3}, S_{-2}, S_{+1} and S_{+2} residues are identical in all members of the family, and the S_{+3} residue is either proline or arginine. As expected, the S_{-1} residue is highly variable as its side chain is fully exposed to solvent. Thus, it seems highly likely that hTRX interacts with and activates all members of this family by specifically reducing the disulfide bond involving the cysteine that is homologous to Cys62 in p50. In contrast, the sequence surrounding the redox-sensitive cysteine in Fos and Jun, which make up the heterodimeric AP-1 transcription factor complex, is entirely different [43]. It is therefore not surprising to find that hTRX alone cannot activate AP-1 DNA binding via cysteine reduction [43].

Biological implications

The activation of a growing number of transcription factors, including NFκB, other members of the Dorsal/Rel family, AP-1, TFIIIC, BZLF1, Myb and p53, is regulated by a thiol–redox control mechanism involving the reduction of a specific cysteine residue by a cellular redox protein. In some cases, such as that of NFκB, the cellular redox protein is human thioredoxin (hTRX) [1–3]; in others, such as AP-1, it is a protein known as Ref-1 [43]. An understanding of the molecular basis of this phenomenon requires the determination of the structures of the cellular redox proteins with their target sites on the various transcription factors.

Activation of the DNA-binding properties of NFκB requires that the cysteine at position 62 of the p50 subunit be reduced [1–3]. The role of Cys62 is readily appreciated in the light of the recently solved crystal structure of a p50 homodimer–DNA complex [28,29] which was reported after our studies were completed. Specifically, the p50 homodimer envelopes the DNA, locking it into a channel. The back of the channel is closed off by the C-terminal dimerization domain of p50, while the front is closed off by two loops, known as L1, one from each subunit. Cys62 is located in the L1 loop. If Cys62 of one subunit is disulfide bridged to Cys62 of the other in uncomplexed NFκB, the DNA can no longer gain access to its binding surface on the p50 homodimer. Likewise, if this disulfide bridge is present in the p50 homodimer–DNA complex, the DNA can no longer be released from the complex.

To understand how hTRX specifically recognizes the L1 loop containing Cys62, we have determined the structure of a mixed disulfide intermediate complex of hTRX with a 13-residue peptide comprising residues 56–68 of the p50 subunit of NFκB. The structure reveals that, in addition to the intermolecular disulfide bridge between Cys32 of hTRX and Cys62 of the NFκB peptide, the complex is stabilized by numerous hydrogen bonding, electrostatic and van der Waals interactions involving residues S_{-5} to S_{+3} (where the S_0 position represents the disulfide-bonded cysteine, Cys62). Interestingly, the S_{-5}(Arg57), S_{-3}(Arg59), S_{-2}(Tyr60), S_0(Cys62) and S_{+1}(Glu63) residues contact the DNA in the p50 homodimer–DNA complex [28,29]. Hence, these residues contribute not only to the specificity of the interaction with hTRX but also to that with DNA. Analysis of these interactions permits one to define the specificity of hTRX-catalyzed disulfide bond reduction. Specifically, the S_{-5} residue should be positively charged, the S_{-3} residue should have a long hydrophobic side chain together with a polar functional group, the side chains of the S_{-4} and S_{+3} residues should be hydrophobic or have a long hydrophobic component, the S_{-2} residue should be hydrophobic, the S_{+1} residue should be hydrophilic, and finally the S_{+2} residue should be small and hydrophobic.

Materials and methods

Sample preparation

The [C35A, C62A, C69A, C73A] mutant of hTRX was constructed using mutagenic oligonucleotides in conjunction with polymerase chain reaction (PCR) technology [44]. All cloning procedures followed standard protocols [45]. The coding sequence was verified by DNA sequencing [46]. Expression and purification of the mutant hTRX was performed by procedures identical to those used previously for the wild-type and [C62A, C69A, C73A] mutant proteins [36,47], and uniform

labeling with either ^{15}N or with ^{15}N and ^{13}C was carried out by growing the bacteria in minimal medium with $^{15}NH_4Cl$ or both $^{15}NH_4Cl$ and $^{13}C_6$-glucose as the sole nitrogen and carbon sources, respectively. It is worth noting that the activity of the triple Cys→Ala mutant protein [C62A, C69A, C73A] in the spectrophotometric insulin reduction assay [48] is the same as that of the wild-type protein [47]. The NFκB peptide $F^{56}RFRYVCEGPSHG^{68}$ was synthesized using solid-phase methods [49] and purified by HPLC using a C4 reversed-phase column. Purity of the peptide was checked by mass spectrometry and NMR spectroscopy. The complex between hTRX and the NFκB peptide was prepared by stirring a reaction mixture containing 0.5 mM hTRX, 1 mM NFκB peptide, 0.016 M cysteamine, 0.009 M cystamine, 94 mM Tris-HCl, pH 8 for 4 h at room temperature, after which time 90% of the hTRX was found to form a mixed disulfide intermediate based on non-reducing SDS-polyacrylamide gel electrophoresis. The complex was then purified on a C4 reversed-phase HPLC column with a 20–70% acetonitrile gradient over 40 min in 0.05% aqueous trifluoroacetic acid. The purified complex was taken up in either 99.996% D_2O or 90% H_2O/10% D_2O in 10 mM sodium phosphate pH 4.4.

NMR spectroscopy

All NMR experiments were carried out at 25°C on either a Bruker AMX600 or AMX500 spectrometer equipped with a z-shielded gradient triple resonance probe. The NMR spectra were processed with the NmrPipe package [50], and displayed and analyzed using the programs PIPP, CAPP and STAPP [51]. The sequential assignment of the ^1H, ^{13}C and ^{15}N chemical shifts, stereoassignments of β-methylene protons and methyl protons of leucine and valine, and the measurement of homonuclear and heteronuclear three-bond coupling constants ($^3J_{HN\alpha}$, $^3J_{\alpha\beta}$, $^3J_{NH\beta}$, $^3J_{COH\beta}$, $^3J_{C\gamma N}$, $^3J_{C\gamma CO}$, $^3J_{CC}$) were achieved using the same set of 2D and 3D heteronuclear experiments previously used in our study of reduced and oxidized hTRX [32]. (Details of these double and triple resonance experiments and original references are provided in reviews [52–54].) The ^1H resonances of the NFκB peptide were assigned by means of the conventional sequential assignment procedure [55,56] using 2D ^{12}C-filtered HOHAHA [57] and $^{12}C(F_1,F_2)$-filtered NOE spectra in D_2O, and $^{14}N/^{12}C(F_1,F_2)$-filtered NOE and $^{14}N(F_2)$-filtered COSY spectra in H_2O [58]. Approximate interproton distance restraints were derived from the following NOE spectra recorded with a mixing time of 120 ms: 2D $^{12}C(F_1,F_2)$-filtered, $^{12}C/^{14}N(F_1,F_2)$-filtered, and $^{14}N(F_2)$-filtered NOE spectra [59]; 3D ^{15}N-edited [60,61], ^{13}C-edited [62,63], and ^{13}C-edited$(F_2)/^{12}C$-filtered(F_3) [64,65] NOE spectra; and 4D $^{15}N/^{13}C$-edited [66] $^{13}C/^{13}C$-edited [67,68] NOE spectra. The interproton distance restraints were grouped into four ranges, 1.8–2.7 Å (1.8–2.9 Å for NOEs involving NH protons), 1.8–3.3 Å (1.8–3.5 Å for NOEs involving NH protons), 1.8–5.0 Å, and 1.8–6.0 Å corresponding to strong, medium, weak and very weak NOEs, respectively [69,70]. Upper distance limits for distances involving methyl protons and non-stereospecifically assigned methylene protons were corrected appropriately for center averaging [71]. In addition, 0.5 Å was added to the upper limit of distances involving methyl protons to account for the higher apparent intensity of methyl resonances [72]. Stereospecific assignments and ϕ, ψ and $\chi1$ torsion angle restraints were obtained using the conformational grid search program STEREOSEARCH [73] on the basis of the $^3J_{HN\alpha}$ and $^3J_{\alpha\beta}$ coupling constants and intra-residue and sequential inter-residue interproton distance restraints involving the NH, CαH and CβH protons. Information from $^3J_{NH\beta}$ and $^3J_{COH\beta}$ coupling constants was also employed for identifying the appropriate $\chi1$ rotamer and for detecting rotamer averaging. $\chi1$ torsion angles for valine and threonine residues and stereospecific assignments for the methyl groups of valine residues were obtained from $^3J_{C\gamma N}$ and $^3J_{C\gamma CO}$ coupling constants, in conjunction with the pattern of intra-residue NOEs. Finally, $\chi2$ torsion angle restraints for isoleucine and leucine residues and stereospecific assignments for the methyl groups of leucine were obtained from $^3J_{CC}$ coupling constants and the pattern of intra-residue NOEs [74]. Stereospecific assignments were obtained for 52 out of the 69 β-methylene groups, and for all methyl groups of the 6 leucine and 11 valine residues of hTRX, and for 5 out of 10 β-methylene groups and for the methyl groups of the single valine residue of the NFκB peptide.

Structure calculations

The structures were calculated using the hybrid distance geometry-simulated annealing protocol [75] which makes use of the program X-PLOR [76]. The target function that is minimized during simulated annealing (SA) comprises only quadratic harmonic potential terms for covalent geometry (that is bonds, angles, planes and chirality), square-well quadratic potentials for the experimental distance and torsion angle restraints, harmonic potentials for the $^3J_{HN\alpha}$ coupling constant [77,78] and $^{13}C\alpha$ and $^{13}C\beta$ secondary chemical shift [79] restraints, and a quartic van der Waals repulsion term for the non-bonded contacts. No hydrogen-bonding, electrostatic or 6–12 Lennard-Jones empirical potential energy terms are present in the target function.

The $^3J_{HN\alpha}$ coupling constants included directly in the refinement comprised only those that could be measured from the 3D HNHA experiment to an accuracy of 0.5 Hz or better. The minimum ranges employed for the ϕ, ψ, $\chi1$ and $\chi2$ torsion angle restraints were $\pm10°$, $\pm50°$, $\pm20°$ and $\pm20°$, respectively [32,78]. The narrow range for some of the ϕ restraints was made possible by the availability of highly accurate $^3J_{HN\alpha}$ coupling constant data. The $\chi2$ angles of all tyrosine and phenylalanine aromatic rings were restrained to $90\pm30°$. In all cases, the angular standard deviations of the torsion angles for the ensemble of 60 final SA structures were much smaller than the ranges employed for the corresponding torsion angle restraints, and all the ϕ,ψ backbone torsion angles lie within the allowed regions of the Ramachandran plot. Only structurally useful intra-residue NOEs were included in the intra-residue interproton distance restraints. Thus, NOEs between protons separated by two bonds or between non-stereospecifically assigned protons separated by three bonds were not incorporated in the restraints. Hydrogen-bonding restraints, which account for all the slowly exchanging backbone amide protons, were only included in the final stages of refinement. The Cα and Cβ secondary shifts restraints include all hTRX residues with the exception of the single cysteine (Cys32), histidine (His44) and tryptophan (Trp31) residues [79].

Simulated annealing with complete cross-validation [80] was carried out on the final set of SA structures. For each simulated annealing run with cross-validation, the data set was randomly partitioned into a test set comprising ~10% of the data and a reference set. Only the latter is included in the target function that is minimized. The test set for each SA structure was therefore different. The atomic rms distribution about the mean coordinate positions remains essentially unchanged upon complete cross-validation and there is no significant shift in the atomic coordinates, that is, the difference between the mean coordinate positions before and after complete cross-validation

(0.11 Å, 0.14 Å and 0.20 Å for backbone atoms, all ordered atoms and all atoms, respectively) is smaller than the rms distribution of the individual structures about the mean coordinate positions. These results indicate the high degree of completeness of the experimental restraints and provide a reliable indication of the accuracy of the structures.

The coordinates of the 60 final simulated annealing (SA) structures of hTRX–NFκB peptide complex, together with the coordinates of the restrained minimized mean structure, $(SA)_r$, and the complete list of experimental NMR restraints and ^1H, ^{15}N, ^{13}C assignments have been deposited in the Brookhaven Protein Data Bank.

Acknowledgements: This work was supported by the AIDS Targeted Anti-Viral Program of the Office of the Director of the National Institutes of Health (GMC, AMG). We thank Dan Garrett and Frank Delaglio for software support, Rolf Tschudin for hardware support, and James Ernst for help in producing the figures.

References

1. Matthews, J.R., Wakasugi, N., Virelizier, J.L., Yodoi, J. & Hay, R.T. (1992). Thioredoxin regulates the DNA binding activity of NF-κB by reduction of a disulfide bond involving cysteine 62. *Nucleic Acids Res.* **20**, 3821–3830.
2. Hayashi, T., Ueno, Y. & Okamoto, T. (1993). Oxidoreductive regulation of nuclear factor κB. *J. Biol. Chem.* **268**, 11380–11388.
3. Mitomo, K., Nakayama, K., Fujimoto, K., Sun, X., Seki, S. & Yamamoto, K. (1994). Two different cellular redox systems regulate the DNA-binding activity of the p50 subunit of NF-κB *in vitro*. *Gene* **145**, 197–203.
4. Toledano, M.B. & Leonard, W.J. (1991). Modulation of transcription factor NF-κB binding activity by oxidation–reduction *in vitro*. *Proc. Natl. Acad. Sci. USA* **88**, 4328–4332.
5. Abate, C., Patel, L., Rauscher, F.J. & Curran, T. (1990). Redox regulation of Fos and Jun DNA-binding activity *in vitro*. *Science* **249**, 1157–1161.
6. Cromlich, J.A. & Roeder, R.G. (1989). Human transcription factor IIIC (TFIIIC). *J. Biol. Chem.* **264**, 18100–18109.
7. Bannister, A.J., Cook, A. & Kouzarides, T. (1991). *In vitro* DNA binding activity of Fos/Jun and BZLF1 but not C/EBP is affected by redox changes. *Oncogene* **6**, 1243–1250.
8. Myrset, A.H., Bostad, A., Jamin, N., Lirsac, P.N., Toma, F. & Gabrielsen, O.S. (1993). DNA and redox state induced conformational changes in the DNA-binding domain of the Myb oncoprotein. *EMBO J.* **12**, 4625–4633.
9. Hainaut, P. & Milner, J. (1993). Redox modulation of p53 conformation and sequence-specific DNA binding *in vitro*. *Cancer Res.* **53**, 4469–4473.
10. Holmgren, A. (1989). Thioredoxin and glutaredoxin systems. *J. Biol. Chem.* **264**, 13963–13966.
11. Holmgren, A. (1984). Enzymatic reduction–oxidation of protein disulfides by thioredoxin. *Methods Enzymol.* **107**, 295–300.
12. Blombäck, B., *et al.*, & Olovson, M. (1974). Enzymatic reduction of disulfide bonds in fibrinogen by the thioredoxin system. I. Identification of reduced bonds and studies on reoxidation process. *Thromb. Res.* **4**, 55–75.
13. Larsson, A., Holmgren, A. & Bratt, I. (1978) Thioredoxin and glutathione in cultured fibroblasts from human cases with 5-oxoprolinuria and cystinosis. *FEBS Lett.* **87**, 61–64.
14. Okada, M., *et al.*, & Yodoi, J. (1985). TCGF (IL-2)-receptor inducing factor(s): II Possible role of ATL-derived factor (ADF) on constitutive IL-2 receptor expression of HTLV-I(+) T cell lines. *J. Immunol.* **135**, 3995–4003.
15. Rinsky, L., *et al.*, & Greene, W.C. (1986). Purification to homogeneity and NH_2-terminal amino acid sequence of a novel interleukin-1 species derived from a human B-cell line. *J. Immunol.* **136**, 3304–3310.
16. Wakasugi, H., *et al.*, & Bertoglio, J. (1987). Epstein–Barr virus-containing B-cell line produces an interleukin-1 that it uses as a growth factor. *Proc. Natl. Acad. Sci. USA.* **84**, 804–808.
17. Tagaya, Y., *et al.*, & Yodoi, J. (1987). Transcription of IL-2 receptor gene is stimulated by ATL-derived factor produced by HTLV-I (+) T cell lines. *Immunol. Lett.* **15**, 221–228.
18. Tagaya, Y., *et al.*, & Yodoi, J. (1989). ATL-derived factor (ADF), an IL-2 receptor/Tac inducer homologous to thioredoxin; possible involvement of dithio-reduction in the IL-2 receptor induction. *EMBO J.* **8**, 757–764.
19. Wakasugi, N., *et al.*, & Tursz, T. (1990). Adult T-cell leukemia-derived factor/thioredoxin, produced by both human T-lymphotropic virus type I and Epstein–Barr virus-transformed lymphocytes, acts as an autocrine growth factor and synergizes with interleukin-1 and interleukin-2. *Proc. Natl. Acad. Sci. USA* **87**, 8282–8286.
20. Deiss, L.P. & Kimchi, A. (1991). A genetic tool used to identify thioredoxin as a mediator of a growth inhibitory signal. *Science* **252**, 117–120.
21. Leung, K. & Nable, G.J. (1988). HTLV-1 transactivator induces interleukin-2 receptor expression through an NF-κB-like factor. *Nature* **333**, 776–778.
22. Lenardo, M.J. & Baltimore, D. (1989). NFκB: a pleiotropic mediator of inducible and tissue-specific gene control. *Cell* **58**, 227–229.
23. Greene, W.C. (1990). Regulation of HIV-1 gene expression. *Annu. Rev. Immunol.* **8**, 453–475.
24. Bauerle, P.A. (1991). The inducible transcription activator NF-κB: regulation by distinct protein subunits. *Biochim. Biophys. Acta* **1072**, 63–80.
25. Bauerle, P.A. & Henkel, T. (1994). Function and activation of NFκB in the immune system. *Annu. Rev. Immunol.* **12**, 141–179.
26. Nabel, G. & Baltimore, D. (1987). An inducible transcription factor activates expression of human immunodeficiency virus in T cells. *Nature* **326**, 711–713.
27. Siekevitz, M., *et al.*, & Greene, W.C. (1987). Activation of the HIV-1 LTR by T cell mitogens and the transactivator protein of HTLV-1. *Science* **238**, 1575–1578.
28. Ghosh, G., Duyne, G.V., Ghosh, S. & Sigler, P.B. (1995). The structure of NFκB p50 homodimer bound to a κB site. *Nature* **373**, 303–310.
29. Müller, G.W., Rey, F.A., Sodeoka, M., Verdine, G.L. & Harrison, S.C. (1995). Structure of the NF-κB homodimer bound to DNA. *Nature* **373**, 311–317.
30. Forman-Kay, J.D., Clore, G.M. & Gronenborn, A.M. (1992). Relationship between electrostatics and redox function in human thioredoxin: characterization of pH titration shifts using two-dimensional homo- and heteronuclear NMR. *Biochemistry* **31**, 3443–3452.
31. Kallis, G.B. & Holmgren, A. (1980). Differential reactivity of the functional sulfhydryl groups of cysteine-32 and cysteine-35 present in the reduced form of thioredoxin from *Escherichia coli*. *J. Biol. Chem.* **255**, 10261–10265.
32. Qin, J., Clore, G.M. & Gronenborn, A.M. (1994). The high-resolution three-dimensional solution structures of the oxidized and reduced states of human thioredoxin. *Structure* **2**, 503–521.
33. Bushweller, F., Åslund, K., Wüthrich & Holmgren, A. (1992). Structural and functional characterization of the mutant *Escherichia coli* glutaredoxin (C14→S) and its mixed disulfide with glutathione. *Biochemistry* **31**, 9288–9293.
34. Bushweller, J.H., Billeter, M., Holmgren, A. & Wüthrich, K. (1994). The nuclear magnetic resonance solution structure of the mixed disulfide between *Escherichia coli* glutaredoxin (C14S) and glutathione. *J. Mol. Biol.* **235**, 1585–1597.
35. Richardson, J.S. (1981). The anatomy and taxonomy of protein structure. *Adv. Protein Chem.* **34**, 167–330.
36. Wollman, E.E., *et al.*, & Fradelizi, D. (1988). Cloning and expression of a cDNA for human thioredoxin. *J. Biol. Chem.* **263**, 15506–15512.
37. Eisenberg, D. & Mclaghlan, A.D. (1986). Solvation energy in protein folding and binding. *Nature* **319**, 199–203.
38. Janin, J. & Chothia, C. (1990). The structure of protein–protein recognition sites. *J. Biol. Chem.* **265**, 16027–16030.
39. Madden, D.R., Gorga, J.C., Strominger, J.L. & Wiley, D.C. (1992). The three dimensional structure of HLA-B27 at 2.1 Å resolution suggests a general mechanism for tight peptide binding to MHC. *Cell* **70**, 1035–1048.
40. Eck, M.J., Shoelson, S.E. & Harrison, S.C. (1993). Recognition of a high-affinity phosphotyrosyl peptide by the Src homology-2 domain of $p56^{lck}$. *Nature* **362**, 87–91.
41. Kumar, S., Rabson, A.B. & Gelinas, C. (1992). The RxxRxRxxC motif conserved in all Rel/κB proteins is essential for the DNA-binding activity and redox regulation of the v-Rel oncoprotein. *Mol. Cell Biol.* **12**, 3094–3106.
42. Toledano, M.B., Ghosh, D., Rrinh, F. & Lennard, W.J. (1993). N-terminal DNA-binding domains contribute to differential DNA-binding specificities of NF-κB p50 and p65. *Mol. Cell Biol.* **13**, 852–860.
43. Xanthoudakis, S., Miao, G.G. & Curran, T. (1994). The redox and DNA-repair activities of Ref-1 are encoded by nonoverlapping domains. *Proc. Natl. Acad. Sci. USA* **91**, 23–27.

44. Sakai, R.K., *et al.*, & Erlich, H.A. (1988). Primer-directed enzymatic amplification of DNA with a thermostable DNA polymerase. *Science* **239**, 487–491.
45. Maniatis, T., Fritsch, E.F. & Sambrook, J. (1994). *Molecular cloning: A Laboratory Manual* (2nd edn). Cold Spring Harbor Laboratory, Cold Spring Harbor, NY.
46. Sanger, F., Nichlen, S. & Coulson, A.R. (1977). DNA sequencing with chain-terminating inhibitors. *Proc. Natl. Acad. Sci. USA* **74**, 5463–5467.
47. Forman-Kay, J.D., Clore, G.M., Stahl, S.J. & Gronenborn, A.M. (1992). ^{1}H and ^{15}N resonance assignments and secondary structure of the human thioredoxin C62A, C69A, C73A mutant. *J. Biomol. NMR* **2**, 431–445.
48. Luthman, M. & Holmgren, A. (1982). Rat liver thioredoxin and thioredoxin reductase: purification and characterization. *Biochemistry* **21**, 6628–6633.
49. Merrifield, R.B. (1963). Solid phase peptide synthesis. I. The synthesis of a tetrapeptide. *J. Am. Chem. Soc.* **85**, 2149–2152.
50. Delaglio, F., Grzesiek, S., Vuister, G., Zhu, G., Pfeifer, J. & Bax, A. (1994). NMRPipe: a multidimensional spectral processing system based on UNIX pipes. Proceedings of the 35th Experimental Nuclear Magnetic Resonance Conference. Abstract No. WP108, p. 262.
51. Garrett, D.S., Powers, R., Gronenborn, A.M. & Clore, G.M. (1991). A common sense approach to peak picking in two-, three- and four-dimensional spectra using automatic computer analysis of contour diagrams. *J. Magn. Reson.* **95**, 214–220.
52. Clore, G.M. & Gronenborn, A.M. (1991). Structures of larger proteins in solution: three- and four-dimensional heteronuclear NMR spectroscopy. *Science* **252**, 1390–1399.
53. Bax, A. & Grzesiek, S. (1993). Methodological advances in protein NMR. *Accounts Chem. Res.* **26**, 131–138.
54. Clore, G.M. & Gronenborn, A.M. (1991). Application of three- and four-dimensional heteronuclear NMR spectroscopy to protein structure determination. *Progr. Nucl. Magn. Reson. Spectrosc.* **23**, 43–92.
55. Wüthrich, K. (1986). *NMR of Proteins and Nucleic Acids.* John Wiley & Sons, New York.
56. Clore, G.M. & Gronenborn, A.M. (1987). Determination of three-dimensional structures of proteins in solution by nuclear magnetic resonance spectroscopy. *Protein Eng.* **1**, 275–288.
57. Bax, A., *et al.*, & Zhu, G. (1994). Measurement of homo- and heteronuclear J couplings from quantitative J correlation. *Methods Enzymol.* **239**, 79–105.
58. Bax, A., Grzesiek, S., Gronenborn, A.M. & Clore, G.M. (1994). Isotope-filtered 2D HOHAHA spectroscopy of a peptide–protein complex using heteronuclear Hartmann–Hann dephasing. *J. Magn. Reson. A* **106**, 269–273.
59. Ikura, I. & Bax, A. (1992). Isotope-filtered 2D NMR of a protein–peptide complex: study of a skeletal muscle myosin light chain kinase fragment bound to calmodulin. *J. Am. Chem. Soc.* **114**, 2433–2440.
60. Marion, D., *et al.*, & Clore, G.M. (1989). Overcoming the overlap in the assignment of ^{1}H-NMR spectra of larger proteins using three-dimensional heteronuclear ^{1}H–^{15}N Hartmann–Hahn and nuclear Overhauser-multiple quantum coherence spectroscopy: application to interleukin-1β. *Biochemistry* **28**, 6150–6156.
61. Zuiderweg, E.R.P. & Fesik, S.W. (1989). Heteronuclear three-dimensional NMR spectroscopy of the inflammatory protein C5a. *Biochemistry* **28**, 2387–2391.
62. Ikura, M., Kay, L.E., Tschudin, R. & Bax, A. (1990). Three-dimensional NOESY-HMQC spectroscopy of a ^{13}C-labeled protein. *J. Magn. Reson.* **86**, 204–209.
63. Zuiderweg, E.R.P., McIntosh, L.P., Dahlquist, F.W. & Fesik, S.W. (1990). Three-dimensional ^{13}C-resolved proton NOE spectroscopy of uniformly ^{13}C-labeled proteins for the NMR assignment and structure determination of larger proteins. *J. Magn. Reson.* **86**, 210–216.
64. Ikura, M., Clore, G.M., Gronenborn, A.M., Zhu, G., Klee, C.B. & Bax, A. (1992). Solution structure of a calmodulin–target peptide complex by multidimensional NMR. *Science* **256**, 632–638.
65. Omichinski, J.G., *et al.*, Gronenborn, A.M. (1993). NMR structure of a specific DNA complex of a Zn-containing DNA-binding domain of GATA-1. *Science* **261**, 438–446.
66. Kay, L.E., Clore, G.M., Bax, A. & Gronenborn, A.M. (1990). Four-dimensional heteronuclear triple-resonance NMR spectroscopy of interleukin-1β in solution. *Science* **249**, 411–414.
67. Clore, G.M., Kay, L.E., Bax, A. & Gronenborn, A.M. (1991). Four-dimensional $^{13}C/^{13}C$-edited nuclear Overhauser enhancement spectroscopy of a protein in solution: application to interleukin 1β. *Biochemistry* **30**, 12–18.
68. Vuister, G.W., *et al.*, & Bax, A. (1993). Increased resolution and improved spectral quality in four-dimensional $^{13}C/^{13}C$-separated HMQC-NOESY-HMQC spectra using pulsed field gradients. *J. Magn. Reson. B* **101**, 210–213.
69. Williamson, M.P., Havel, T.F. & Wüthrich, K. (1985). Solution conformation of proteinase inhibitor IIA from bull seminal plasma by ^{1}H nuclear magnetic resonance and distance geometry. *J. Mol. Biol.* **182**, 295–315.
70. Clore, G.M., Nilges, M., Sukumaran, D.K., Brünger, A.T., Karplus, M. & Gronenborn, A.M. (1986). The three-dimensional structure of α1-purothionin in solution: combined use of nuclear magnetic resonance, distance geometry and restrained molecular dynamics. *EMBO J.* **5**, 2729–2735.
71. Wüthrich, K., Billeter, M. & Braun, W. (1983). Pseudo-structures for the 20 common amino acids for use in studies of protein conformations by measurements of intramolecular proton–proton distance constraints with nuclear magnetic resonance. *J. Mol. Biol.* **169**, 949–961.
72. Clore, G.M., Gronenborn, A.M., Nilges, M. & Ryan, C.A. (1987). Three-dimensional structure of potato carboxypeptidase inhibitor in solution: a study using nuclear magnetic resonance, distance geometry, and restrained molecular dynamics. *Biochemistry* **26**, 8012–8023.
73. Nilges, M., Clore, G.M. & Gronenborn, A.M. (1990). ^{1}H-NMR stereospecific assignments by conformational data-base searches. *Biopolymers* **29**, 813–822.
74. Powers, R., Garrett, D.S., March, C.J., Frieden, E.A., Gronenborn, A.M. & Clore, G.M. (1993). The high resolution three-dimensional solution structure of human interleukin-4 determined by multidimensional heteronuclear nuclear magnetic resonance. *Biochemistry* **32**, 6744–6762.
75. Nilges, M., Clore, G.M. & Gronenborn, A.M. (1988). Determination of three dimensional structures of proteins from interproton distance data by hybrid distance geometry-dynamical simulated annealing calculations. *FEBS Lett.* **229**, 317–324.
76. Brünger, A.T. (1992). *X-PLOR Version 3.1: A System for X-ray Crystallography and NMR.* Yale University, New Haven, CT.
77. Garrett, D.S., Kuszewski, J., Hancock, T., Vuister, G.W., Gronenborn, A.M. & Clore, G.M. (1994). The impact of direct refinement against three-bond HN-CαH coupling constants on protein structure determination by NMR. *J. Magn. Reson. B* **104**, 99–103.
78. Lodi, P.J., *et al.*, & Clore, G.M. (1994). High resolution solution structure of the β chemokine hMIP-1β by multidimensional NMR. *Science* **263**, 1762–1767.
79. Kuszewski, J., Qin, J., Gronenborn, A.M. & Clore, G.M. (1995). The impact of direct refinement against $^{13}C\alpha$ and $^{13}C\beta$ chemical shifts on protein structure determination by NMR. *J. Magn. Reson. B* **106**, 92–96.
80. Brünger, A.T., Clore, G.M., Gronenborn, A.M., Saffrich, R. & Nilges, M. (1994). Assessing the quality of solution nuclear magnetic resonance structure by complete cross-validation. *Science* **261**, 328–331.
81. Brooks, B.R., Bruccoleri, R.E., Olafson, B.D., States, D.J., Swaminathan, S. & Karplus, M. (1983). CHARMM: a program for macromolecular energy minimization and dynamics calculations. *J. Comput. Chem.* **4**, 187–217.
82. Delano, W. & Brünger, A.T. (1993). *AVS-X-PLOR User's Manual.* Yale University, New Haven, CT.
83. Nicholls, A.J. (1993). *GRASP Manual.* Columbia University, New York.
84. De Castro, E. & Edelstein, S. (1992). *VISP 1.0 User's Guide.* University of Geneva, Switzerland.
85. Kraulis, P.J. (1991). MOLSCRIPT: a program to produce both detailed and schematic plots of protein structures. *J. Appl. Crystallogr.* **24**, 946–950.

Received: **11 Jan 1995**; revisions requested: **2 Feb 1995**; revisions received: **6 Feb 1995**. Accepted: **8 Feb 1995**.